To cite this version :

Camille LOYER, Paulo FERREIRA, Jean-Baptiste MARIJON, Vincent MICHEL, Julie VERA, Vincent DUVAL, Gilles REGNIER, Emmanuel RICHAUD - Embrittlement of polybutylene terephthalate induced by injection molding - Polymer Degradation and Stability - Vol. 196, p.109843 - 2022

Embrittlement of polybutylene terephthalate induced by injection molding

C. Loyer [a,b], P. Ferreira [a], J-B. Marijon [a], V. Michel [a], G. Régnier [a], J. Vera [b], V. Duval [b], E. Richaud [a,*]

[a] PIMM Laboratory, Arts et Métiers Institute of Technology, CNRS, Cnam, HESAM Université, 151 Boulevard de l'Hôpital, 75013 Paris, France
[b] APTIV, Z.I des Longs Réages, 28230 Epernon, France

ABSTRACT

Embrittlement caused by injection molding was investigated on a commercial grade of Polybutylene terephthalate (PBT). The effect of temperature and residence time in the barrel on mechanical properties was studied. Results were discussed from macromolecular analysis by Gel Permeation Chromatography and crystallinity measurements by differential scanning calorimetry. It was shown that embrittlement exclusively occurs by a chain scission process in those conditions. Oxygen is shown to play a negligible role in degradation while thermolysis seems to be the main source of degradation. It was here described by a first simple kinetic model based on the beta abstraction of hydrogen at the vicinity of ester groups. A processing window was thus determined using this model and might help practitioners for processing PBT parts.

Keywords:
Injection molding
Processing window
Embrittlement
Degradation
Kinetic modeling
PBT

1. Introduction

Polybutylene Terephthalate (PBT) is an engineering thermoplastic that can be easily processed by injection molding since its melting temperature is in principle much lower than its degradation temperature [1]. It is well accepted that mechanical properties of resulting materials depend on the processing conditions (melt temperature [2,3], mold temperature [3], cooling time [4]. In the case of injection molding, barrel temperature and screw speed in the case of extrusion [5]). Many previous papers report the effect of the processing conditions and of the processing induced morphology on mechanical properties of glass fibers PBT [6–8].

The residence time in the case of injection, or number of cycles in the case of extrusion [9] also induce changes in mechanical properties. It was actually previously shown that PBT becomes brittle when its molar mass becomes lower than a critical value (M'$_{wc}$) which depends on crystallinity[10]. Nevertheless, this critical value M'$_{wc}$ seems close to the (initial) molar mass value corresponding to common PBT grades for injection purposes [10]. PBT undergoes mostly chain scissions either under hydrolytic or thermal aging (in presence or absence of oxygen), both modes of aging

being, *a priori,* possible in processing conditions [11] and it is noteworthy that the degradation mechanisms occurring in the case of injection molding is not known at now.

End of life criteria (for the failure in tensile mode) were previously established in the case of thin films submitted either to humid or thermo-oxidative aging, but the representativeness of those criteria remains to be validated for bulky material, submitted to various kinds of mechanical loadings (tensile tests at various elongation rate, notched impact…) [12].

Moreover, the degradation kinetics are not known for PBT in the molten state, which is a mandatory condition to define a "time-temperature" map for processing, and develop a kinetic model for describing the occurrence of chain scission in the processing conditions, as it was for example done in the case of PET recycling [11].

The aims of the present paper are hence:

- to link residual mechanical properties of PBT parts with processing conditions;
- to valid the end of life criteria obtained on thin films on bulk materials "closer" to PBT injection molded products;
- to identify a "processing window" time temperature for neat PBT (antioxidant free) and develop a first kinetic model for describing degradation in molten state.

Table 1
Barrel temperatures and residence times for processing samples.

Samples	Barrel temperature (°C)	Cycle time (s)	Residence time (min)
1	240	22.4	4
2	240	84.1	16
3	240	123	24
4	260	78.5	16
5	280	22.1	4
6	280	74.2	16
7	280	113	24

2. Experimental

2.1. Materials

The PBT under study was a common injection grade (M_n = 38.3 kg/mol, M_w = 82.8 kg/mol, Polydispersity Index PDI = 2), which was processed with parameters given in Table 1. Its initial Oxidation Onset Temperature (OOT) was measured as illustrated in Appendix (see Figure SI-1). Dumb-bell samples (illustrated in Figure SI-2 with the following dimensions length: l_1 = 80 mm, l_2 = 108 mm, l_3 = 47.5 mm, h = 4 mm, b_1 = 10 mm, b_2 = 20 mm) were processed using a DK Codim 175/140 injection machine having a diameter screw of 36 mm, a maximum shot capacity at 185 cm^3 and a clamping force of 175 tons. Injection temperatures were chosen as 240 and 260 °C as typical temperatures for processing PBT (see [6] for example) and 280 °C as an extreme temperature which can be encountered in cases where very thin parts are processed and the solidification in contact with cold mold want to be avoided. Processing times were chosen so as to observe various level of degradation.

Prior to injection molding, PBT resin was dried at least 4 h at 120 °C with a DR30H from Engin Plast Due. Measurements of residual water amount with FLV type Hydrotracer from Aboni confirmed that the pellets were below the maximum level required by the manufacturer (0.04%) so that hydrolysis occurring during the injection molding process can be neglected in the following.

The residence time in the barrel was calculated as followed:

$$Residence\ time = \frac{Melted\ volume}{Melted\ shift} \times cycle\ time \tag{1}$$

where the melted volume and melted shift are respectively equal to 321 cm^3 and 29.8 cm^3. The corresponding cycle times are given in Table 1.

2.2. Sample characterization

2.2.1. Mechanical testing

Before any mechanical testing, the dumb-bell specimens were placed at least 24 h in a desiccator at 50%RH and 23 °C following the ISO 291 standard.

2.2.1.1. Tensile tests.
Uniaxial tensile testing was performed on dumb-bell specimens at room temperature using an INSTRON 5581 machine with a 5 kN cell with elongation rates equal to 0, 50 and 100 mm/min. Mechanical extensometer was used during the tests in the elastic area only.

2.2.1.2. Charpy impact test.
Impact tests were carried out on Impact tester from CEAST on dumb-bell samples. Samples were prepared following the norm ISO 179–1. The notches were made with a type C notcher. The dimensions of the notch were verified by taking pictures with optical microscope (not shown here). The notch depth was measured at 1.8 mm which is in agreement with the ISO 179–1 standard. The hammer energy was equal to 2 J and hammer speed to 30 m/s.

2.2.2. Differential scanning calorimetry

Morphological changes were followed by calorimetric measurements with a DSC Q1000 supplied by TA Instruments. Prior to any measurement, DSC apparatus was calibrated with an indium standard. About 6–8 mg of PBT sealed in standard aluminum pans were subjected to a heating ramp from 30 °C to 250 °C followed by a cooling ramp from 250 °C to 0 °C. Both cycles were performed at 10 °C/min rate.

The mass crystallinity χ_c was determined from the melting peak enthalpy ΔH_f measurement using a 100% crystalline PBT melting enthalpy $\Delta H_f°$ of 141 J/g [13,14] according to the following equation:

$$\chi_c = 100 \left(\frac{\Delta H_f}{\Delta H_f°} \right) \tag{2}$$

Results were analyzed using TA Analysis software.

2.2.3. Gel permeation chromatography

Gel permeation chromatography (GPC) were performed by PeakExpert Laboratory (Tours, France) based on a detailed experiment given in [10]. PBT samples were dissolved in Hexafluoroisopropanol (HFiP) with 0.1 M potassium trifluoride (KTFA) at 2.0 g/L. The injection volume was 50 μL at 1 mL/min at 40 °C. The measurements were performed on a Waters e2695 apparatus equipped with a RID Waters 2414 refractometer. Three columns were used: PFG 10 μm, 1000 Å, ID 8.0 mm × 100 mm; PFG 10 μm, 1000 Å, ID 8,0 mm × 300 mm and PFG 10 μm, 100 Å, ID 8.0 mm × 300 mm. The post-treatment was done by using PSS-WinGPC Unity software. Molar masses were given as PMMA equivalent.

2.2.4. Thermogravimetric analysis

The thermogravimetric tests were made on a Q50 apparatus from TA Instruments with Aiolos GasMix instrument from Alytech allowing mixing nitrogen and oxygen. About 6 mg of material placed on a platinum pan were heated at a 10 °C/min rate up to 280 °C under nitrogen and then isothermally maintained under various under various O_2–N_2 mixture (21, 10, 5% oxygen pressure and pure nitrogen).

2.2.5. Fourier transformed infrared spectroscopy

Measurements have been performed on pellets and dumb-bells with a Frontier device (Perkin-Elmer) in ATR mode equipped with a diamond crystal. 16 scans were acquired between 650 and 4000 cm^{-1} at a 4 cm^{-1} resolution.

2.2.6. Wide angle X ray scattering

The X-ray analysis was conducted on a PANalytical X'Pert diffractometer equipped with a Philips PW3040 X Ray generator, a Göbel mirror (divergence: 0.02° in the incident beam optics), and a X'Celerator real time multiple strip detector. A tube with a copper anode was used emitting mainly through the K_α ray at a wavelength of 0.154 nm. The 2θ diffraction data were collected from 5° up to 110° with a step of 0.05° with an integrated acquisition time of 300 s. Fixed anti-scatter and divergence slits of 0.04 rad were used together with a beam mask of 10 mm. All scans were carried out in the so-called continuous mode.

Two samples were analyzed in reflection: the surface of the sample and the surface after removing 300 μm by mechanical polishing were scanned. Grazing incidence X-ray diffraction provides a powerful method for determining the structure of the surface region of a polymer. By varying the angle of incidence of the X-ray beam, the penetration depth can be tuned to allow a direct comparison of molecular ordering in the surface. A grazing angle of 3° to probe the near surface on the first 60 μm was chosen according to the master curve showed in Fig. 1.
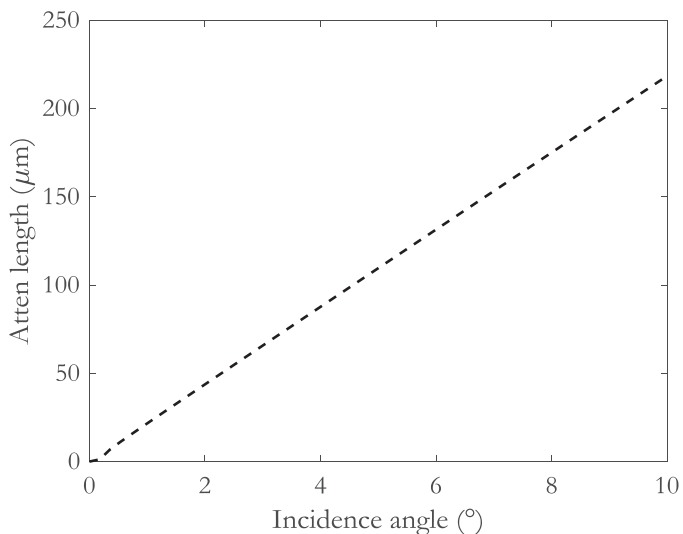
Fig. 1. Master curved of beam penetration versus incidence angle.

3. Results and discussion

3.1. Mechanical tests

Fig. 2 depicts the typical (average) stress stain curves of samples processed with various barrel temperatures and residence times (recalled in Table 1). Those latter do not modify neither the elastic domain nor the yield stress (which is about 55 MPa, in line with previously observed values [15]).

Fig. 2a indicates that increasing either barrel temperature or residence time results in a decrease of elongation at break (the minimal, maximal, averages values are given in SI, together with standard deviation). However, the disappearance of plastic deformation is only visible at 280 °C with a residence time of 16 min and 24 min. One can also note from Fig. 2b that the possible degradation induced by injection process does not significantly affect neither the Young's modulus nor the yield stress (NB: consistently with other recent examples illustrating the effect of crystallinity on PBT storage [16] or modulus average molar mass and crystalline ratio on POM yield stress [17]).

In order to establish the link between processing conditions and residual mechanical properties, ultimate elongations were plotted for various processing conditions (Fig. 3). As already illustrated by Barba et al. [18], the decrease of elongation rate induces an increase of elongation at break. This is clearly visible for samples processed with the lowest barrel temperature. This is also visible for samples processed at 260 °C - 16 min and 280 °C - 4 min but in a lower extent. For samples processed at 280 °C - 16 and 24 min, the effect is hardly visible suggesting that, irrespectively of deformation rate, degradation level is too important to allow any plastic deformation and can be considered as ductile considering the embrittlement criterion previously established [10,19], i.e. $\varepsilon_{R,c} < \varepsilon_{R,0}/2$, eR,0 being here higher than respectively 150, 200 and 350% for the samples respectively tested at 10, 50 and 100 mm/min,

In the aim to verify if the effect of proceedings conditions can be generalized to other mechanical properties, Charpy impact tests were also performed. Data are presented in Fig. 4 (the minimal, maximal, averages values are given in SI, together with standard deviation). The obtained values for the less degraded material (240 °C – 4 min) are on the same order of magnitude than those obtained by other authors [20–22], with differences possibly coming from chosen experimental parameters (hammer speed and energy). The effect of processing parameters is almost the same

than for ultimate elongation: it seems that 3 groups can be distinguished: the "non-degraded ones" (processed at 240 °C), the very degraded ones (280 °C-16 min and 280 °C-24 min) and an intermediate family (260 °C – 16 min) and 280 °C – 4 min. Interestingly, for this last family, it seems that impact resistance remains closer to the "non-degraded family" (contrarily to tensile tests) suggesting that a given level of degradation (at macromolecular scale) has more effect on ultimate elongation.

3.2. Macromolecular changes

To better understand the mechanical behavior of injected PBT samples, characterization of polymer at macromolecular scale was carried out in order to discuss the loss of plastic deformation in terms of structure properties relationships.

As previously discussed [10,19], mechanical properties of semicrystalline polymers (in particular the existence of plastic behavior, and cracking resistance) depend on molar mass value, this latter decreasing possibly due to chain scissions occurring during the processing stage and being evidenced from the decrease of average weight molar mass and average number molar mass, M_w and M_n respectively. We used Saito's equation to determine the concentration in chain scissions (s) and crosslinking (x) [23]. Contribution of chain condensation might be taken into account since a polycondensation reaction (cond) counterbalances a chain scission, it can be written:

$$\frac{1}{M_w} - \frac{1}{M_{w0}} = \frac{s - cond}{2} - 2x \quad (4)$$

$$\frac{1}{M_n} - \frac{1}{M_{n0}} = (s - cond) - x \quad (5)$$

Average molar mass values are given in Table 2 together with the estimation for chain scissions and crosslinking concentrations.

Table 2 shows that (s-cond) >> x and hence $s >> x$ meaning that injection molding mainly leads to random chain scissions phenomenon. It is well in line with the fact that PDI index remains around 2.2 regardless the barrel temperature or the residence time.

It is actually expected that shorter chain (produced by processing induced degradation) can crystallize more easily [19] which explains why crystallinity increases (Table 2).

It is noteworthy that crystallinity measurements represent an average value for the whole sample thickness, as suggested from previous studies showing as crystallinity on the sample thickness. Other studies show the existence of a crystallinity profile in the thickness, with the existence of amorphous external layers, meanwhile crystallinity increases in the deeper layer [24]. To check this hypothesis, polarized optical microscopy analyses were carried out on the two extreme families corresponding in terms of processing conditions: 240 °C – 4 min and 280 °C – 24 min (Fig. 5).

Fig. 5 shows the well-known skin-core phenomenon observed by Hobbs and Pratt [24] for PBT. It was previously observed that both the increase of barrel temperature and residence time lead to crystallinity and crystallization temperature increase (see Table 2). The skin thicknesses are roughly equal to 150 µm and 140 µm for 240 °C – 4 min and 280 °C – 24 min respectively.

The transparency of the skin layer could be interpreted as follows: (i) the skin layer is amorphous or (ii) the crystallite size is smaller than the visible wavelength. Here WAXS measurements (Fig. 6) performed using a 3° incidence angle (i.e. 60 µm deep) allow the skin layer to be analyzed and clearly show its crystalline nature for both injection molding conditions (240 °C – 4 min and 280 °C – 16 min). One can note that the 2θ angles are similar to the one obtained in previous studies [25,26] on PBT. Bragg's angles are identical for the skin and the core layer indicating that crystallinity should be the same. It can be pointed out that peaks
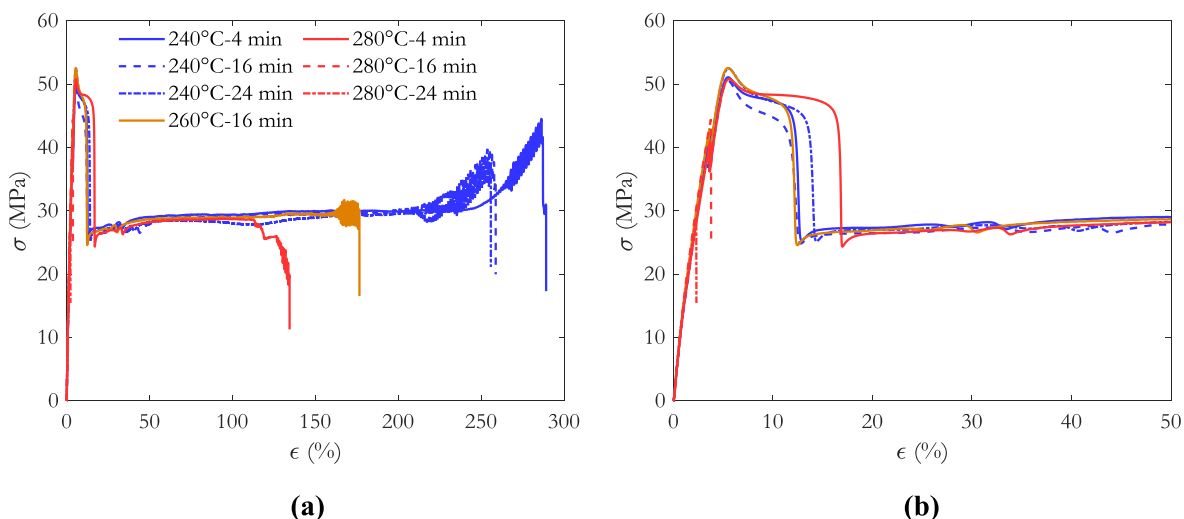
Fig. 2. Stress-strain curves on dumb-bell samples for the seven injection molding families conditions for PBT (a) and zoom in the low deformation zone (b).

Table 2
Changes in weight molar masses and crystallinity on dumb-bell (s and x were obtained using Eqs. (4) and (5) with M_{n0} = 38.3 kg/mol and M_{w0} = 82.8 kg/mol).

Name	M_n (kg/mol)	M_w (kg/mol)	PDI	χ_C (%)	s-cond (mol/kg)	x (mol/kg)
(mol/kg)						
240 °C – 4 min	34.0	77.5	2.3	35.5	3.85×10^{-3}	5.50×10^{-4}
240 °C – 16 min	33.6	72.7	2.2	33.6	3.75×10^{-3}	9.88×10^{-5}
240 °C – 24 min	31.4	68.4	2.2	37	5.95×10^{-3}	2.17×10^{-4}
260 °C – 16 min	27.6	59.4	2.2	38.5	1.03×10^{-2}	2.02×10^{-4}
280 °C – 4 min	30.6	66.9	2.2	37	6.85×10^{-3}	2.76×10^{-4}
280 °C – 16 min	19.2	42.8	2.2	39	2.71×10^{-2}	1.13×10^{-3}
280 °C – 24 min	14.3	32.6	2.3	40.5	4.60×10^{-2}	2.18×10^{-3}
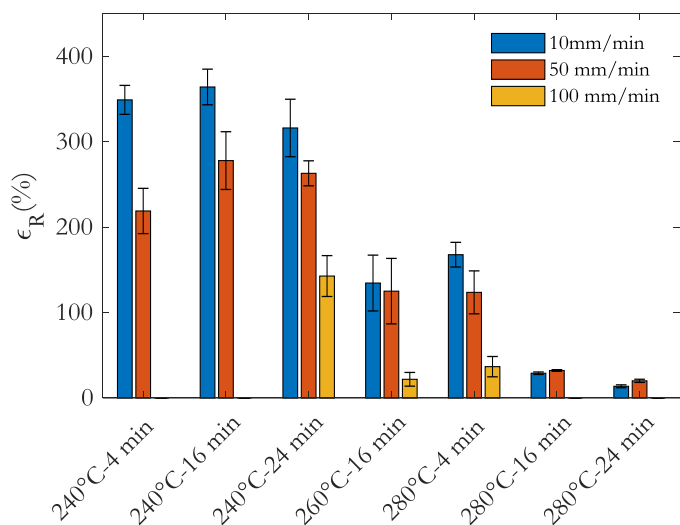
Fig. 3. Average values and average standard deviation of elongation at break values of PBT.
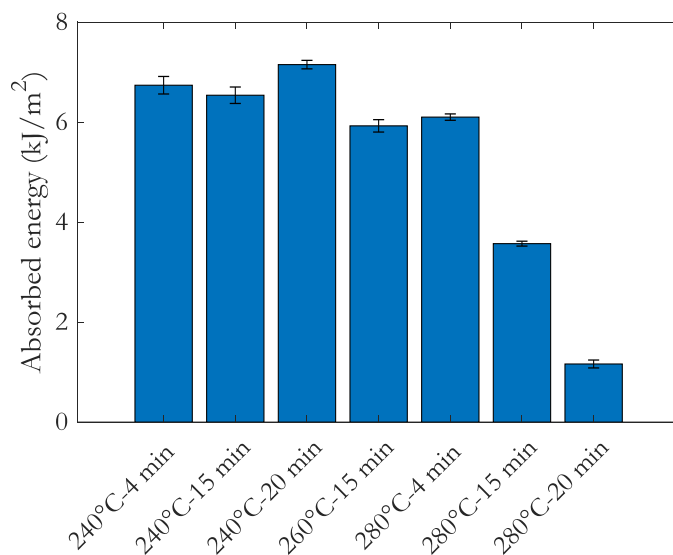
Fig. 4. Absorbed energy average and average standard deviation of PBT.

for the skin layer in the 240 °C – 4 min sample are less defined than the ones measured at 300 μm for the sample molded in the same condition. It could mean distance between diffracted planes is less regular leading to less perfect crystals. This result is confirmed with DSC measurement (not shown here).

According to Fig. 7, despite different processing conditions, the melting temperature remained unchanged. However, the crystallization temperature is slightly higher after 24 min at 280 °C (186 °C for pellet vs 193 °C after 24 min at 280 °C). The crystal-

lization temperature increase could be attributed to the presence of shorter chains coming from chain scissions process which have a higher crystallization temperature.

Those data were placed on the previously embrittlement map established for thermally and hydrolytically aged films, where two domains are distinguished: the domain of ductile samples (high molar mass, low crystalline ratio) and the domain of brittle samples (low molar mass and high crystalline ratio). Here the comparison of aged films and bulky processed samples allow verify-
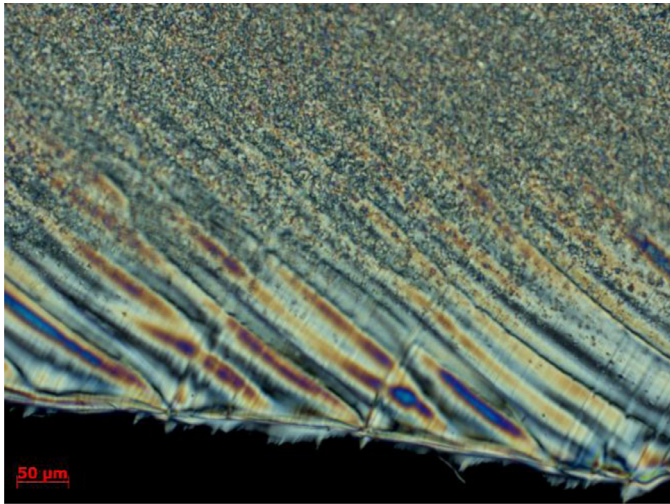
(a)
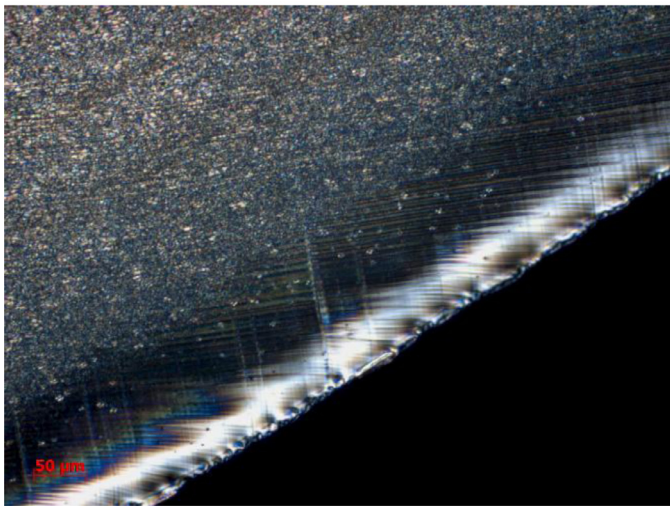
(b)

Fig. 5. Polarized optical microscopy of 240 °C – 4 min (a) and 280 °C – 24 min (b) at x20 magnification.
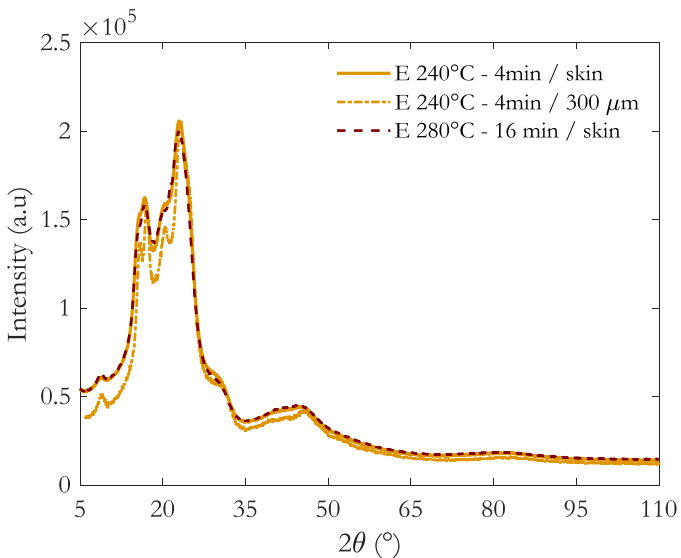

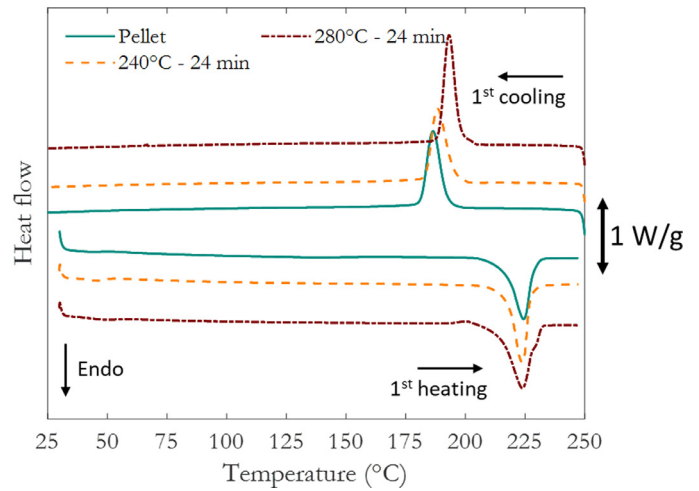**Fig. 6.** WAXS profile of dumb-bell specimens processed with the various conditions.

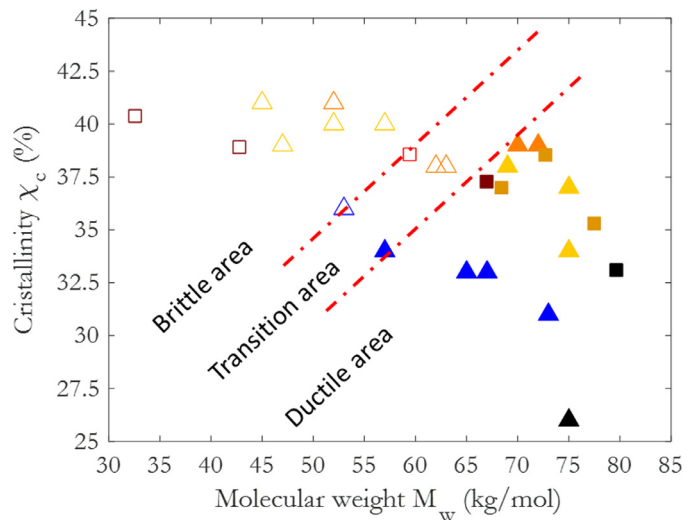**Fig. 7.** Thermograms of PBT pellet (straight line), and PBT processed with various conditions.

Fig. 8. Embrittlement map for PBT based on previous study at 180 °C and 210 °C[10] and hydrolysis at 80 °C(▲, △) and after injection molding (■, □). Filled forms (▲, ■) are ductile and open one are brittle (△, □).

ing the universality of the ductile/brittle transition. Results given in Fig. 8 are in line with our previous results according to which PBT plasticity can be predicted from a $\chi_{c}-M_w$ map with two domains corresponding to ductile (high weight molar mass, low crystallinity ratio) and brittle behavior [10]. It means that the embrittlement criterion proposed for thin films is still valid for bulky materials, which are closed to industrial material. According to Fig. 3, it seems also that the frontier is slightly shifted when changing the solicitation rate.

3.3. Chemical degradation

The aim of this last section is to propose a mechanistic explanation for the here above results, so as to derive a kinetic model allowing to predict the processing induced degradation as a function of time and temperature.

Previous studies on PBT degradation [27,28] showed that using an elevated processing temperature leads to chain scissions. Some groups characteristic of the oxidative degradation were previously identified by Rivaton [29]. According to Fig. 9, it seems that even the most degraded samples (280 °C-20 min) do not display the expected degradation products, suggesting that (i) either they are
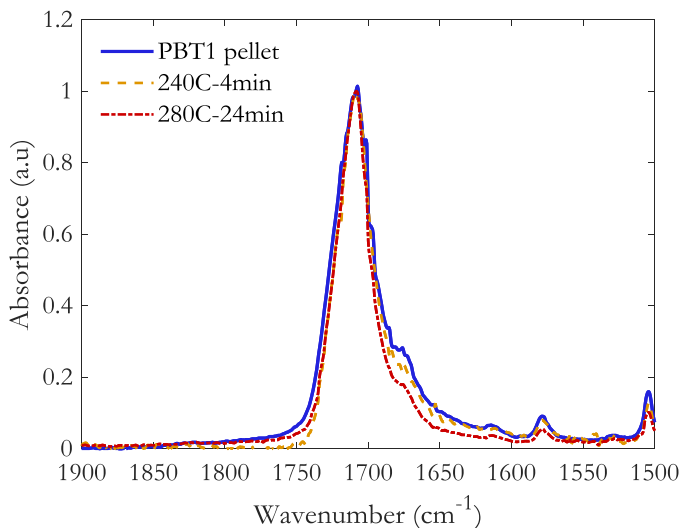
Fig. 9. FTIR-ATR spectra in the carbonyl region of PBT pellet (−), and PBT processed and PBT processed with various conditions.
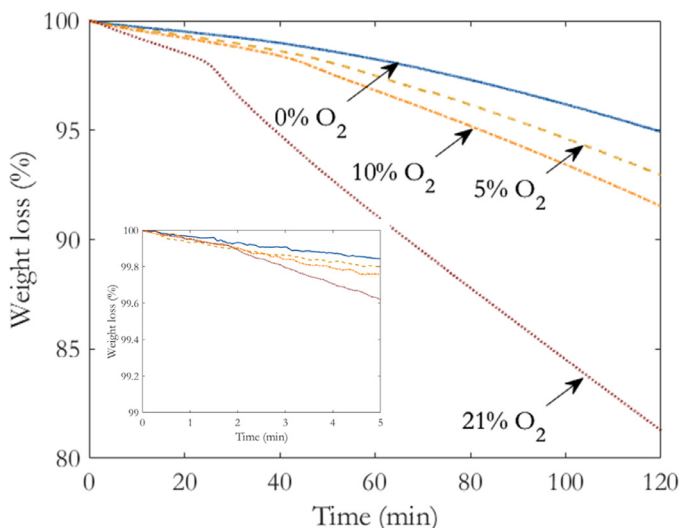

Fig. 10. Weight loss versus exposure time under several oxygen partial pressures.

formed but are instable in the processing conditions or (ii) that the degradation mechanism does not involve oxygen. This is in fact not surprising. A recent paper also illustrates that the carbonyl absorption band is hardly modified even in case where hydrolysis induces significant changes in the hydroxyl region [30].

To better understand the nature of the degradation mechanism, TGA were carried out under several oxygen partial pressures (Fig. 10). It can be first recalled that in case of PET thermal degradation, oxygen hardly modifies the changes in degradation kinetics. Indeed, Nait-Ali et al. study about PET thermal-oxidation at 280 °C [11] show that degradation takes place on a much longer time than those studied here. Regarding processing window, typically less than 5 min, viscosity changes are insignificant regardless the oxygen rate during their experiment: less than 1% change at 0.1% and 9% O_2 rate.

According to TGA measurements (Fig. 10) at 280 °C at 10 °C/min, degradation rate (in terms of mass loss) is hardly modified by the presence of oxygen for moderate times (about 20 min, which correspond to the timescale under investigation in the present work). More precisely, mass loss curves at 280 °C are very close for samples aged under inert atmosphere, 5 and 10%

O_2. It seems hence that degradation is mainly a purely thermolytic process.

Another way to verify the previously established hypothesis is to compare experimental values obtained for molar mass changes with the ones obtained by Gervat [31] under nitrogen. Experimental values of molar mass (Table 2) were plotted versus time and compared with data given by the M_n values derived from the iso-conversion lines. At each temperature under investigation, experimental data obtained in this work match quite well with data obtained for a thermolytic degradation.

In other words, even if oxygen in present in the processing conditions, its contribution seems to be negligible. A first kinetic model for thermolysis (in absence of oxygen) will hence be proposed in the next paragraph.

3.4. Kinetic modeling

Under the assumption that thermal oxidation is negligible, there are a priori 3 reactions likely to modify the molar mass values

① Thermal decomposition of repetitive unit $PH \rightarrow s + alkene$ (k_d)

② Irregularities decomposition $Irreg \rightarrow RCOOH + alkene + S$ (k_i)

③ Condensation $RCOOH + ROH \rightarrow RCOOCOR + H_2O - s$ (k_c) where pH is associated to CH methylene bond, RCOOH a carboxylic acid, s a chain scission, RCOOCOR an anhydride and ROH an alcohol. k_c for polycondensation values were can be estimated from literature about polycondensation and post-polycondensation of PEN [32], PET [33–35] and PBT [36–39]. They are summarized in Table 3:

One can note there is two outliers values from Fortunato et al. [38] and Gostoli et al. [39] on Fig. 11(a). These higher values could be due to catalysts effects, but this remains to be evidenced.

Considering those values found in literature, it suggests that k_c should be between than 10^{-4} and 10^{-3} L/mol/s (1.65×10^{-4} L/mol/s at 215 °C [37]) at 280 °C. In other words, the maximal condensation rate would be about 5.14×10^{-6} mol/L/s at 280 °C calculated with the following formula:

$$condensation\ rate = k_c \times \left(\frac{1}{M_{n,0}}\right)^2 \tag{6}$$

where k_c is the condensation rate and $M_{n,0}$ the initial number molar mass (meaning that chain ends are in concentration equal to $1/M_{n0}$). It will be seen later that it seems to play a minor influence on molar mass changes.

Let us focus on the reactions responsible for chain scissions. Under the assumption that molar mass decrease only originates from the thermal decomposition of irregularities (such as chain ends, weak entanglement, intra lamellar defect), Eq. (4) becomes:

$$\frac{1}{M_n} - \frac{1}{M_{n,0}} = [Irreg] - [condensation] \tag{7}$$

So that

$$[Irreg] > \frac{1}{M_w} - \frac{1}{M_{w,0}} \tag{8}$$

According to data reported in Fig. 12, it suggests that initial irregularities concentration about 0.23 mol/L which would represent about [Irreg] $\times M_m/\rho \sim 5\%$ of structural irregularities. This is considerably higher than PET case where Nait-Ali et al. considered that impurities represents 0.05% in the monomer batch and is for us not physically acceptable.

It suggests that another reaction takes place leading to chain scission. Based on literature [27,28], it seems that PBT thermolysis also leads to the formation of alkene ends chains. This reaction

Table 3
Rate constants for polycondensation based on literature.

References	[32]	[33]	[34]	[36]	[37]	[38]	[39]
Rate constant	3.5×10^{-4} L/mol/s	1.4×10^{-3} L/mol/s	5.0×10^{-4} L/mol/s	4.8×10^{-3} L/mol/s	1.7×10^{-3} L/mol/s	6.6×10^{-3} L/mol/s	7.6×10^{-4} L/mol/s
Temperature	280 °C	275 °C	280 °C	Extrapolation at 280 °C	280 °C	200 °C	220 °C
Catalyst	Yes	No	Yes	Yes	Yes	Yes	Yes
Polymers	PEN	PET	PET	PBT	PBT	PBT	PBT

(a)   **(b)**
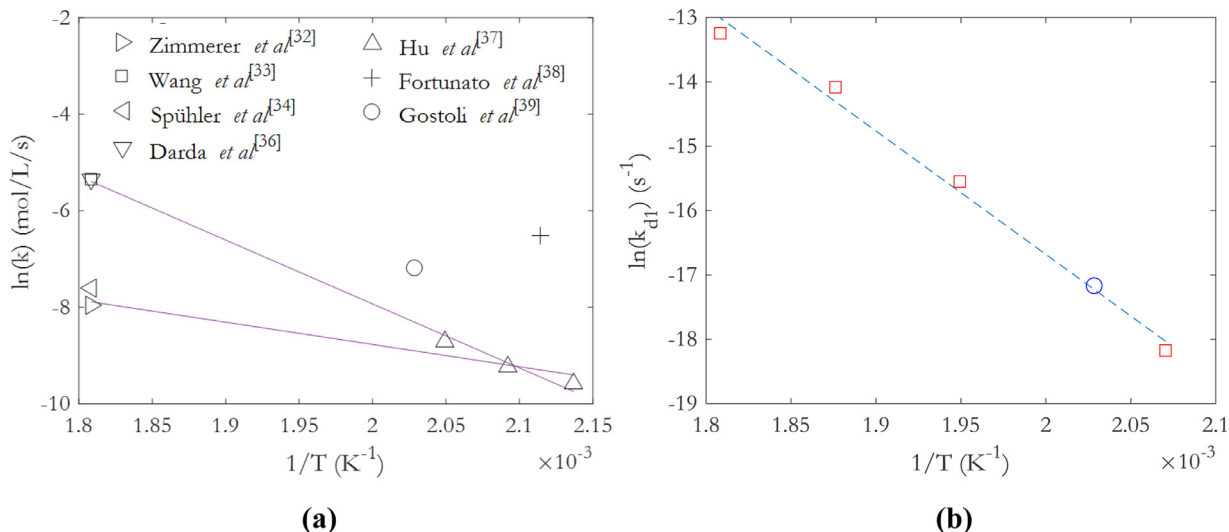
Fig. 11. Arrhenius plots for k_c from literature data (see Table 3) (a) and for k_{d1} extracted from Fig. 14 (□) and literature [38] (○) (b).
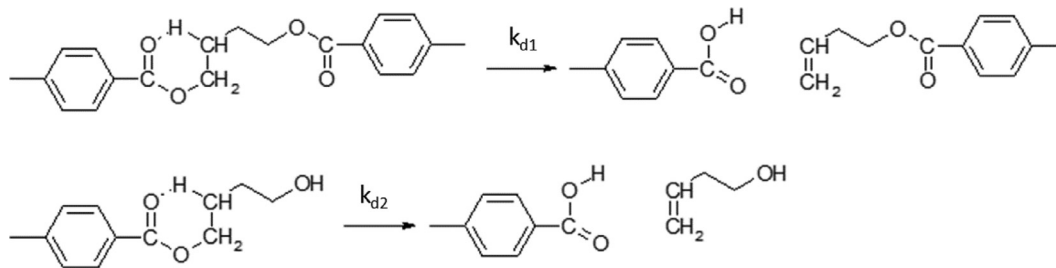
Scheme 1. Proposed degradation pathway.
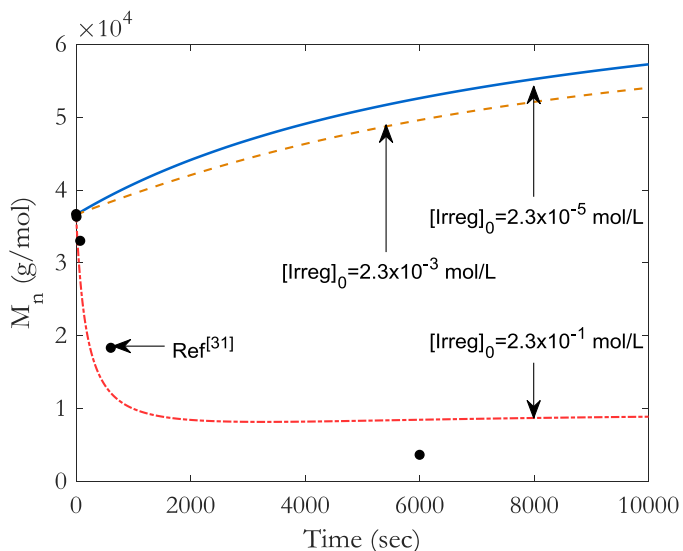
Fig. 12. Simulations with several initial irregularities concentrations and comparisons with literature data [31].

could actually occur either at chain ends or in random positions of chains (Scheme 1):

Taking into account all those considerations, the following model was considered:

$$P_1H \rightarrow RCOOH + s \ (k_{d1})$$

$$ROH \rightarrow RCOOH \ (k_c)$$

Carboxylic end groups (RCOOH, either initially present, or formed during the d1 and d2 reactions) can also condensate:
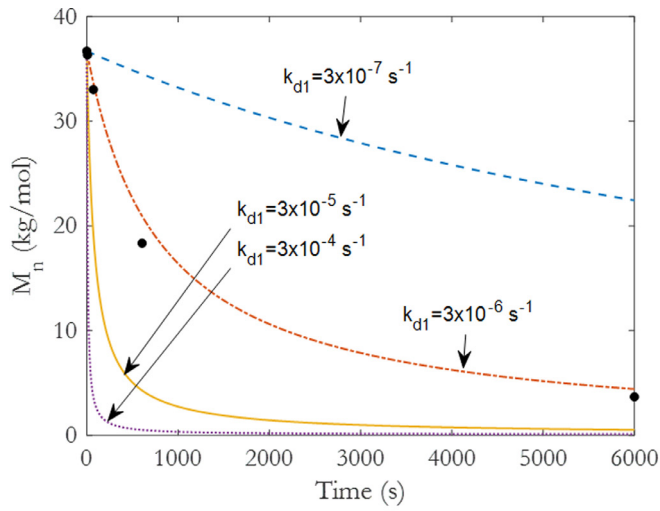
$$ROH + RCOOH \rightarrow cond \ (k_c)$$
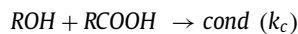
The following differential system is thus expected to describe the degradation of PBT at molten state in absence of oxygen:
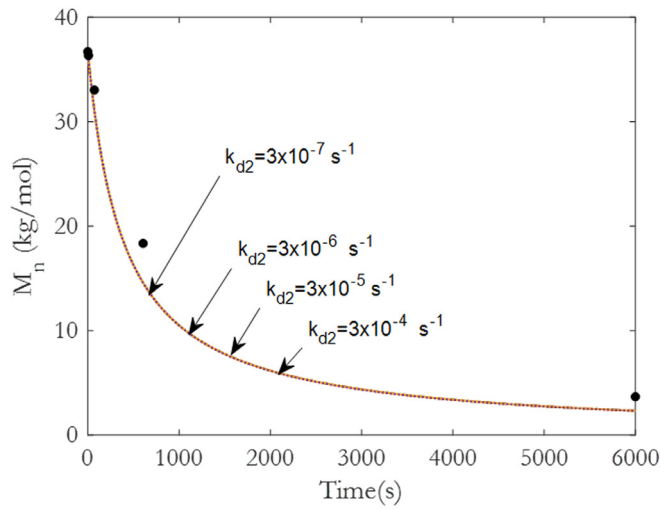
$$\frac{d[RCOOH]}{dt} = k_{d1}[P_1H] + k_{d2}[ROH] - k_C[RCOOH][ROH] \quad (9)$$

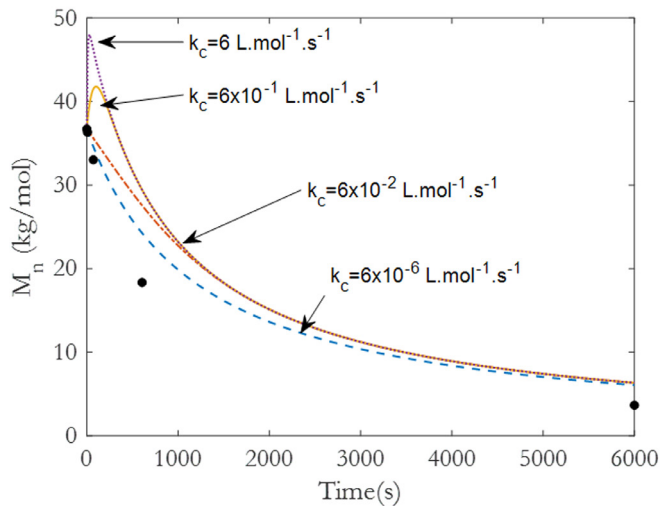$$\frac{d[ROH]}{dt} = -k_{d2}[ROH] - k_C[RCOOH][ROH] \quad (10)$$

$$\frac{d[cond]}{dt} = k_C[RCOOH][ROH] \quad (11)$$

Fig. 13. Parametric study at 280 °C and comparison of the model with literature data.

$$\frac{ds}{dt} = k_{d1}[P_1H] \qquad (12)$$

The concentration in thermolyzable groups located in the middle of chains is increased for each condensation reaction so that

$$\frac{d[P_1H]}{dt} = -k_{d1}[P_1H] + k_C[RCOOH][ROH] \qquad (13)$$

Last, the changes in molar mass are given by Eq. (4) so that

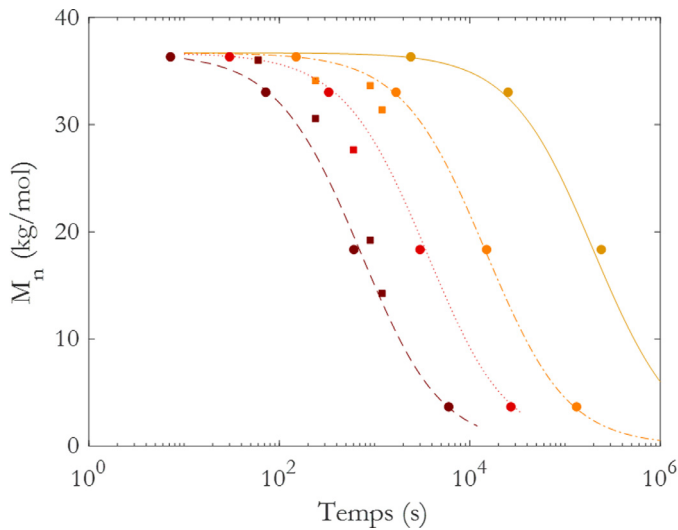$$\frac{dM_n}{dt} = -k_{d1}[P_1H]M_n^2 + k_C[RCOOH][ROH]M_n^2 \qquad (14)$$

Fig. 14. Kinetic modeling of literature (●) [31] and experimental data obtained in this work (■), at 210 °C (-), 240 °C(-.-), 260 °C (..) and 280 °C(–).
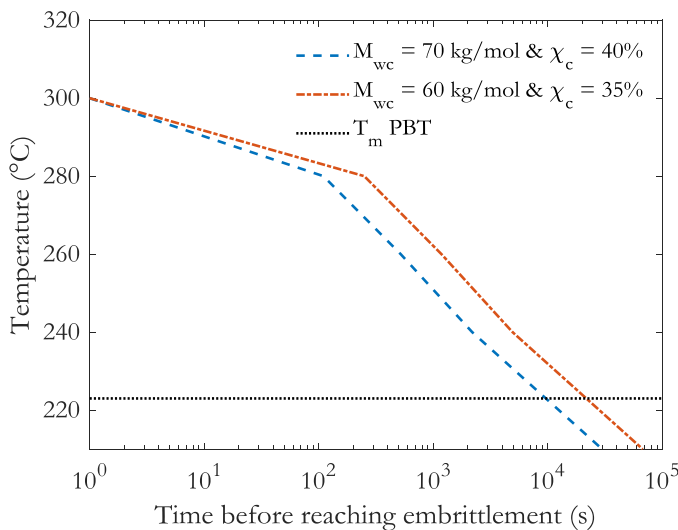

Fig. 15. Processing map for PBT in the absence of oxygen.

This differential system can be solved using ODE23s Matlab tool with the following initial conditions:

$$[RCOOH]_0 = [ROH]_0 = \frac{1}{M_{n0}} \tag{16}$$

$$s_{(t=0)} = cond_{(t=0)} = 0 \tag{17}$$

$$[P_1H]_0 = \frac{2\rho}{M_m} - \frac{1}{M_{n0}} \tag{18}$$

$$M_n = M_{n0} \tag{19}$$

According to a parametric study (Fig. 13) it can be seen that:

– k_{d2} (for chain ends) has a very low influence compared to k_{d1}, as long as $k_{d1} > 3 \times 10^{-6} \times k_{d2}$, consistently with the matter that chain ends are in low concentration compared to other reactive groups
– the polycondensation effects are not observed apart if k_c is higher than 6×10^{-1} L/mol/s which is out of the range of values compiled in Fig. 11a.

It means that thermolysis events occurring randomly in the chains predominate. Therefore, using data from [31], acceptable fits of overall data are obtained (Fig. 14) leading to a first estimation of rate constant for several temperatures (Fig. 11b). Our values fit well with a value given in [38] justifying the physical sense of the proposed model. The activation energy can be estimated at for k_{d1}: $E_{d1} = 221.9$ kJ/mol and the pre-exponential factor at 4.14×10^{11} s^{-1} (see Fig. 11b) which is the expected order of magnitude for an order 1 reaction. The activation energy is very consistent with data obtained for "pure" thermal degradation processes [40,41].

It seems to us interesting to compare it with apparent values for oxidation processes (about 200 kJ/mol [42]). According to this comparison, thermal degradation would predominate at high temperature but would be negligible at low temperature (typically in solid state) where oxidation processes become mostly responsible of PBT failure.

Using both embrittlement map and injected PBT degradation modeling, a processing window for neat PBT has been established and exhibited on Fig. 15.

One must note that when the ideal processing time will be established, the time to obtain a well-melted PBT has to be taken into account. Decreasing the residence time allows limiting degradation and mechanical properties loss but rheological issues could affect mechanical properties.

4. Conclusions

This paper describes the effect of PBT processing on mechanical properties. Samples were injected for various conditions differing by temperature and residence time. Residual plasticity decreased when increasing the processing temperature. Those changes were discussed in terms of residual molar mass and crystalline ratio, which allowed the embrittlement map previously established for PBT films to be confirmed. At temperatures just above the melting point, PBT can be processed without risk of embrittlement. However, if temperature is increased, the risk to get brittle parts becomes more and more important. The use of recycled parts with lower initial molar mass value also increases this possibility.

The discussion of molecular aspects responsible for molar mass changes results in neglecting oxidation in a first approach for injection molding. Hence, those results were used to propose a kinetic model for PBT thermolysis helping practitioners to design a processing map.

It would be interesting to complete the process map with additional considering the PBT hydrolysis [43]. The possibility to broaden this processing map by chain extenders and or hydrolysis retardants such as diazocarbodimides [44] or epoxide by products [45] is also of interest for manufacturers and would offer to scientist the possibility to complete the proposed kinetic models. At last, we stress on the fact that the embrittlement of manufactured PBT parts (during aging and/or in service conditions) also strongly depends on the geometry and its interplay with processing conditions [46] which must be taken into account into future research.

Declaration of Competing Interest

We hereby confirm that we have no conflict of interest with the paper

CRediT authorship contribution statement

C. Loyer: Data curation, Formal analysis, Investigation, Writing – original draft, Writing – review & editing. **P. Ferreira:** Investigation. **J-B. Marijon:** Investigation, Writing – original draft. **V. Michel:** Investigation, Writing – original draft. **G. Régnier:** Conceptualization, Funding acquisition, Methodology, Project administration, Su-

Acknowledgments

Supplementary material

Supplementary material associated with this article can be found, in the online version, at doi:10.1016/j.polymdegradstab. 2022.109843.

References

[1] F. Li, et al., Thermal degradation and their kinetics of biodegradable poly(butylene succinate-co-butylene terephthate)s under nitrogen and air atmospheres, Polym. Deg. Stab. 91 (8) (2006) 1685–1693, doi:10.1016/j. polymdegradstab.2005.12.005.

[2] U.A. Dar, Y.J. Xu, S.M. Zakir, M.-.U. Saeed, The effect of injection molding process parameters on mechanical and fracture behavior of polycarbonate polymer, J. Appl. Polym. Sci. 134 (7) (Feb. 2017), doi:10.1002/app.44474.

[3] M. Feldmann, The effects of the injection moulding temperature on the mechanical properties and morphology of polypropylene man-made cellulose fibre composites, Compos. Part A 87 (2016) 146–152, doi:10.1016/j.compositesa. 2016.04.022.

[4] E. Farotti, M. Natalini, Injection molding. Influence of process parameters on mechanical properties of polypropylene polymer. A first study, Procedia Struct. Integr. 8 (2018) 256–264, doi:10.1016/j.prostr.2017.12.027.

[5] Y. Ding, C. Abeykoon, Y.S. Perera, The effects of extrusion parameters and blend composition on the mechanical, rheological and thermal properties of LDPE/PS/PMMA ternary polymer blends, Adv. Ind. Manuf. Eng. 4 (2022) 100067, doi:10.1016/j.aime.2021.100067.

[6] M.B. Baradi, C. Cruz, and G. Régnier, 'Mechanical characterization of frontal and flowing weld lines in injection-molded short fiber-reinforced thermoplastics', Dresden, Germany, 2019, p. 070009. doi: 10.1063/1.5084853.

[7] M.B. Baradi, C. Cruz, T. Riedel, G. Régnier, Mechanical and microstructural characterization of flowing weld lines in injection-molded short fiber-reinforced PBT, Polym. Test. 74 (2019) 152–162, doi:10.1016/j.polymertesting.2018.12.017.

[8] M.B. Baradi, C. Cruz, G. Régnier, T. Riedel, Microstructural characterization of frontal and flowing weld lines in injection molded short fiber reinforced thermoplastics, Presented at the 18th European Conference on Composite Materials, ECCM, 2018.

[9] C. Freymond, A. Guinault, C. Charbuillet, B. Fayolle, Reprocessing of polymer blends from WEEE: a methodology for predicting embrittlement, Polym. Test. 106 (2022) 107458, doi:10.1016/j.polymertesting.2021.107458.

[10] C. Loyer, G. Régnier, V. Duval, Y. Ould, E. Richaud, PBT plasticity loss induced by oxidative and hydrolysis ageing, Polym. Deg. Stab. 181 (2020) 109368, doi:10. 1016/j.polymdegradstab.2020.109368.

[11] L.K. Nait-Ali, X. Colin, A. Bergeret, Kinetic analysis and modelling of PET macromolecular changes during its mechanical recycling by extrusion, Polym. Deg. Stab. 96 (2) (2011) 236–246, doi:10.1016/j.polymdegradstab.2010.11.004.

[12] S. Hashemi, Fracture of polybutylene terephthalate (PBT) film, Polymer (43) (2002) 4033–4041.

[13] K. Jariyavidyanont, R. Androsch, C. Schick, Crystal reorganization of poly (butylene terephthalate), Polymer 124 (2017) 274–283, doi:10.1016/j.polymer.2017. 07.076.

[14] C. Fosse, et al., Determination of the equilibrium enthalpy of melting of two-phase semi-crystalline polymers by fast scanning calorimetry, Thermochim. Acta 677 (2019) 67–78, doi:10.1016/j.tca.2019.03.035.

[15] M.B. Baradi, C. Cruz, T. Riedel, G. Régnier, Frontal weld lines in injection-molded short fiber-reinforced PBT: extensive microstructure characterization for mechanical performance evaluation, Polym. Compos. 40 (12) (2019) 4547–4558, doi:10.1002/pc.25310.

[16] C.J.F. Braz, J.R.M. Silva, R.M.R. Wellen, M.S. Rabello, The investigation of the stress cracking behavior of PBT by acoustic emission, Polym. Adv. Technol. 32 (12) (2021) 4787–4804, doi:10.1002/pat.5470.

[17] R. Song, M. Berer, A. Muliana, Mechanical responses of Semi-crystalline thermoplastic polymers at various temperatures, Int. J. Solids Struct. 238 (2022) 111398, doi:10.1016/j.ijsolstr.2021.111398.

[18] D. Barba, Temperature and strain rate dependences on hardening and softening behaviours in semi-crystalline polymers: application to PEEK, Int. J. Solids Struct. 182–183 (2020) 205–217.

[19] O. Okamba-Diogo, E. Richaud, J. Verdu, F. Fernagut, J. Guilment, B. Fayolle, Investigation of polyamide 11 embrittlement during oxidative degradation, Polymer 82 (2016) 49–56, doi:10.1016/j.polymer.2015.11.025.

[20] S. Arai, S. Tsunoda, A. Yamaguchi, T. Ougizawa, Effects of short-glass-fiber content on material and part properties of poly(butylene terephthalate) processed by selective laser sintering, Addit. Manuf. 21 (2018) 683–693, doi:10.1016/j. addma.2018.04.019.

[21] A. Cecere, R. Greco, G. Ragosta, G. Scarinzi, A. Taglialatela, Rubber toughened polybutylene terephthalate: influence of processing on morphology and impact properties, Polymer 31 (7) (1990) 1239–1244, doi:10.1016/0032-3861(90) 90214-J.

[22] L. Niu, et al., Influence of nano-Sb_2O_3 particles on mechanical properties of PBT flame retardant composites, Ferroelectrics 546 (1) (2019) 148–157, doi:10. 1080/00150193.2019.1592467.

[23] O. Saito, Effects of high energy radiation on polymers II. End-linking and gel fraction, J. Phys. Soc. Japan 13 (1958) 1451–1464.

[24] S.Y. Hobbs, C.F. Pratt, The effect of skin-core morphology on the impact fracture of poly(butylene terephthalate), J. Appl. Polym. Sci. 19 (6) (1975) 1701–1722, doi:10.1002/app.1975.070190621.

[25] G.S. Deshmukh, D.R. Peshwe, S.U. Pathak, J.D. Ekhe, Nonisothermal crystallization kinetics and melting behavior of poly(butylene terephthalate) (PBT) composites based on different types of functional fillers, Thermochim. Acta 581 (2014) 41–53, doi:10.1016/j.tca.2014.02.007.

[26] K.R. Gorda, D.G. Peiffer, Properties of sulfonated poly(butylene terephthalate), J. Polym. Sci. B 30 (3) (1992) 281–292, doi:10.1002/polb.1992.090300308.

[27] F. Samperi, C. Puglisi, R. Alicata, G. Montaudo, Thermal degradation of poly(butylene terephthalate) at the processing temperature, Polym. Deg. Stab. 83 (1) (Jan. 2004) 11–17, doi:10.1016/S0141-3910(03)00167-8.

[28] G. Montaudo, C. Puglisi, F. Samperi, Primary thermal degradation mechanisms of Poly(ethylene terephthalate) and Poly(butylene terephthalate), Polym. Deg. Stab. 42 (1) (1993) 13–28, doi:10.1016/0141-3910(93)90021-A.

[29] A. Rivaton, Photochemistry of poly(butyleneterephthalate): 2–Identification of the IR-absorbing photooxidation products, Polym. Deg. Stab. 41 (3) (1993) 297–310, doi:10.1016/0141-3910(93)90076-U.

[30] C.S.P. Borges, et al., Effect of water ingress on the mechanical and chemical properties of polybutylene terephthalate reinforced with glass fibers, Materials 14 (5) (2021) 1261, doi:10.3390/ma14051261.

[31] L. Gervat, Structure, propriétés mécaniques et renforcement au choc du PBT, 2001.

[32] W. Zimmerer, E. Amhred, D. Zierer, A. Renken, The influence of mass transfer on polycondensation kinetics, ECCE1, Florence, 1997.

[33] Y. Wang, S. Chen, S. Guang, Y. Wang, X. Zhang, W. Chen, Continuous post-polycondensation of high-viscosity poly(ethylene terephthalate) in the molten state, J. Appl. Polym. Sci. 136 (19) (2019) 47484–47496, doi:10.1002/app.47484.

[34] C. Spühler, W. Zimmerer, A. Renken, Microgravimetric determination of poly-condensation kinetics, DECHEMA Monographs 134 (1998) 587–595.

[35] T. Rieckmann, S. Völker, Micro-kinetics and mass transfer in poly(ethylene terephthalate) synthesis, Chem. Eng. Sci. 56 (3) (2001) 945–953, doi:10.1016/ S0009-2509(00)00309-2.

[36] P.J. Darda, J.A. Hogendoorn, G.F. Versteeg, F. Souren, Reaction kinetics of poly-butylene terephthalate polycondensation reaction, AIChE J 51 (2) (Feb. 2005) 622–630, doi:10.1002/aic.10360.

[37] L. Hu, L. Wu, F. Song, B.-.G. Li, Kinetics and modeling of melt polycondensation for synthesis of poly[(butylene succinate)-co-(butylene terephthalate)], 1 – Esterification.pdf', Macromol. React. Eng. 4 (9–10) (2010) 621–632.

[38] B. Fortunato, F. Pilati, P. Manaresi, Solid state polycondensation of poly(butylene terephthalate), Polymer 22 (1981) 655–657.

[39] C. Gostoli, F. Pilati, G.C. Sarti, B. Di Giacomo, Chemical kinetics and diffusion in poly(butylene terephthalate) solid-state polycondensation: experiments and theory, J. Appl. Polym. Sci. 29 (9) (1984) 2873–2887, doi:10.1002/app.1984. 070290917.

[40] J.M. Encinar, J.F. González, Pyrolysis of synthetic polymers and plastic wastes. Kinetic study, Fuel Process. Technol. 89 (7) (2008) 678–686, doi:10.1016/j. fuproc.2007.12.011.

[41] A. Niksiar, A.H. Faramarzi, M. Sohrabi, Kinetic study of polyethylene terephthalate (PET) pyrolysis in a spouted bed reactor, J. Anal. Appl. Pyrol. 113 (2015) 419–425, doi:10.1016/j.jaap.2015.03.002.

[42] E. Richaud, X. Colin, B. Fayolle, L. Audouin, J. Verdu, Induction period in the low-temperature thermal oxidation of saturated hydrocarbons: example of polyethylene, Int. J. Chem. Kinet. 40 (12) (2008) 769–777, doi:10.1002/kin. 20347.

[43] C. Loyer, G. Régnier, V. Duval, E. Richaud, Multiscale study of poly(butylene terephthalate) hydrolysis, Polym. Degrad. Stab. 192 (2021) 109690, doi:10.1016/ j.polymdegradstab.2021.109690.

[44] A. Bardin, P.-Y.Le Gac, S. Cérantola, G. Simon, H. Bindi, B. Fayolle, Hydrolytic kinetic model predicting embrittlement in thermoplastic elastomers, Polym. Deg. Stab. 171 (2020) 109002, doi:10.1016/j.polymdegradstab.2019.109002.

[45] L.G. Santos, L.C. Costa, L.A. Pessan, Development of biodegradable PLA/PBT nanoblends, J. Appl. Polym. Sci. 135 (12) (2018) 45951, doi:10.1002/app.45951.

[46] D. Dobrotă, S.V. Lazăr, Redesign of the geometry of parts produced from PBT composite to improve their operational behavior, Polymers 13 (15) (2021) 2536–2560, doi:10.3390/polym13152536.